



Diffusing-wave spectroscopy: dynamic light scattering in the multiple scattering limit

D.J. Pine, D.A. Weitz, J.X. Zhu, E. Herbolzheimer

► To cite this version:

D.J. Pine, D.A. Weitz, J.X. Zhu, E. Herbolzheimer. Diffusing-wave spectroscopy: dynamic light scattering in the multiple scattering limit. *Journal de Physique*, 1990, 51 (18), pp.2101-2127. 10.1051/jphys:0199000510180210100 . jpa-00212514

HAL Id: jpa-00212514

<https://hal.science/jpa-00212514>

Submitted on 4 Feb 2008

HAL is a multi-disciplinary open access archive for the deposit and dissemination of scientific research documents, whether they are published or not. The documents may come from teaching and research institutions in France or abroad, or from public or private research centers.

L'archive ouverte pluridisciplinaire **HAL**, est destinée au dépôt et à la diffusion de documents scientifiques de niveau recherche, publiés ou non, émanant des établissements d'enseignement et de recherche français ou étrangers, des laboratoires publics ou privés.

Classification
Physics Abstracts
05.40

Diffusing-wave spectroscopy : dynamic light scattering in the multiple scattering limit

D. J. Pine, D. A. Weitz, J. X. Zhu and E. Herbolzheimer

Exxon Research and Engineering, Route 22 East, Annandale, New Jersey 08801

(Received on January 3, 1990, accepted in final form on May 16, 1990)

Abstract. — Dynamic light scattering is extended to optically thick (opaque) media which exhibit a very high degree of multiple scattering. This new technique, called diffusing-wave spectroscopy (DWS), exploits the diffusive nature of the transport of light in strongly scattering media to relate the temporal fluctuations of the multiply scattered light to the motion of the scatterers. A simple theory of DWS, based on the diffusion approximation for the transport of light, is developed to calculate the temporal electric field autocorrelation functions of the multiply scattered light. Two important scattering geometries are treated : transmission and backscattering. The theory is compared to experimental measurements of Brownian motion of submicron-diameter polystyrene spheres in aqueous suspension. The agreement between theory and experiment is excellent. The limitations of the photon diffusion approximation and the polarization dependence of the autocorrelation functions are discussed for the backscattering measurements. The effects of absorption of light and particle polydispersity are also incorporated into the theory and verified experimentally. It is also shown how DWS can be used to obtain information about the mean size of the particles which scatter light.

1. Introduction.

Dynamic light scattering (DLS) has proven to be a powerful tool for the study of dynamical processes in simple and complex fluids. Using photon correlation techniques to analyze the temporal fluctuations of scattered light, DLS provides detailed information about the dynamics of the scattering medium [1, 2, 3]. A significant limitation of DLS (also called quasielastic light scattering or photon correlation spectroscopy) has been the lack of a general scheme for applying it to systems which exhibit strong multiple scattering. However, in a series of recent experiments, DLS has been extended to study optically thick media which exhibit a very high degree of multiple scattering [4, 5, 6]. This new technique, called diffusing wave spectroscopy (DWS), exploits the diffusive nature of the transport of light in strongly scattering media to relate the temporal fluctuations of multiply scattered light to the motion of the scatterers. Thus, DWS can be used to study particle motion in concentrated fluids such as colloids, microemulsions, and other systems which are characterized by strong multiple scattering [6, 7]. The basic features of DWS have been outlined previously in brief reports by

several groups [4, 5, 6]. Here, we present a more extensive report on the theoretical and experimental details of DWS.

Before the development of DWS there were numerous attempts to account for the effects of multiple scattering in DLS experiments. Most focused on systems which exhibit relatively weak multiple scattering. The most successful of these techniques, developed by Phillies [8] and Dhont *et al.* [9] rely on elaborate schemes which discriminate against multiply scattered light so that only the fluctuations of singly scattered light are analyzed. These techniques are practical, however, only when a significant fraction of the scattered light which is collected has been scattered just once. By contrast, DWS relates the temporal fluctuations of *multiply scattered light* to the underlying dynamics of the scattering medium. Thus, DWS extends the application of conventional DLS to strongly scattering systems which are completely dominated by multiple scattering, that is, to systems which are essentially opaque.

One important consequence of multiple scattering is that DWS probes particle motion over length scales much shorter than the wavelength of light in the scattering medium, λ . This is to be contrasted with DLS in the single scattering limit, where the characteristic time dependence of the fluctuations is determined by particle motion over a length scale set by the inverse wavevector $q^{-1} \sim \lambda$, where $q = (4\pi/\lambda) \sin(\theta/2)$ and θ is the scattering angle. In the multiple scattering regime, the characteristic time dependence is determined by the cumulative effect of many scattering events and, thus, by particle motion over length scales much less than λ . Therefore, the characteristic time scales are much faster and the corresponding characteristic length scales are much shorter than for conventional DLS.

In the following section we review the theory of DWS based on the diffusion approximation for the transport of light. We then apply this theory to two important experimental geometries, backscattering and transmission, and compare the predictions of the theory to experimental measurements on aqueous colloidal suspensions of polystyrene spheres. We also discuss the limitations of the photon diffusion approximation for describing the transport of light within the context of our backscattering measurements. In subsequent section, we show how DWS can be used for particle sizing, and discuss the effects of absorption of light and particle polydispersity.

2. Theory.

The key to the theory of DWS is the description of the propagation of light in a multiply-scattering medium in terms of the diffusion approximation. Within this approach, the phase correlations of the scattered waves within the medium are ignored, and only the scattered intensities are considered [10]. Thus, the path followed by an individual photon can be described as a random walk. Whether the diffusion approximation is valid in a given system depends on the length scales over which the transport of light is described. For length scales less than the mean free path (or extinction length), ℓ , of the coherent field, the wave equation for the electric field must be used. For length scales longer than ℓ , the phase correlation of the waves must be considered only for limited, specialized cases. The most commonly studied example is that of enhanced backscattering where the phase coherence of the scattered fields plays an essential role [11, 12]. More generally, it is only in the case of extremely strong scattering, where the Ioffe-Regel limit is approached, and light localization is predicted to occur, that the use of the full wave equation is essential [13]. However, achieving this criterion has proven elusive and, for nearly all cases of practical interest, the transport of light can be described in terms of the intensity or energy density.

For scatterers much smaller than λ , the scattering from each particle is isotropic and the direction of the light propagation is randomized by a single scattering event or, equivalently,

over a distance ℓ . In this case the transport of the light energy density, $U(\mathbf{r}, t)$, can be described over length scales longer than ℓ by the diffusion equation

$$\frac{\partial}{\partial t} U(\mathbf{r}, t) = D_\ell \nabla^2 U(\mathbf{r}, t), \quad (2.1)$$

where D_ℓ is the diffusion coefficient of the light. Then, $D_\ell = c\ell/3$ where c is the speed that the light travels through the effective background medium. For particles which are not small compared to λ , the scattering is anisotropic, and the mean number of scattering events, n_0 , required to randomize the direction of light propagation is greater than one. The length scale over which this randomization occurs is the transport mean free path, ℓ^* , defined by $\ell^* = n_0 \ell$. Thus, for $n_0 > 1$, the diffusion equation is valid only over length scales longer than ℓ^* and $D_\ell = c\ell^*/3$. In practice, this means that the theory for DWS based solely on the diffusion approximation will provide an accurate description of the temporal fluctuations of the scattered light when the sample dimensions are greater than ℓ^* and the distance that photons travel through the sample is much greater than ℓ^* .

Two theoretical approaches have been used to describe the fluctuations in the scattered electric field. The first approach starts from the wave equation for the propagation of light and uses a diagrammatic expansion to describe the scattering from random fluctuations in the dielectric constant. The lowest order term in this expansion corresponds to the diffusion approximation. The consequences of motion of the scatterers were first considered by Golubentsev [14] and temporal autocorrelation functions for different scattering geometries were calculated by Stephen [15]. Subsequently, MacKintosh and John [16] refined this approach by considering the effects of anisotropic scatterers and non-diffusive modes of propagation of the light.

The second theoretical approach differs from the first by considering the diffusive transport of individual photons directly, rather than starting from the wave equation. The path of each photon is determined by random, multiple scattering from a sequence of particles. The fluctuations in the phase of the electric field due to the motion of the scatterers is calculated for each light path. The contributions of all paths, appropriately weighted within the photon diffusion approximation, are then summed to obtain the temporal autocorrelation function. It is mathematically simpler and physically more transparent than diagrammatic methods. It can also be more easily generalized to larger particles which scatter light anisotropically. This approach was first developed by Maret and Wolf [4] to analyze temporal correlation functions of light backscattered from dense colloidal suspensions. Pine *et al.* [6] extended their analysis to transmission geometries and calculated explicit expressions for the correlation functions. This work was recently reviewed by Pine *et al.* [17]. In section 2.A, we follow the earlier works of Maret and Wolf [4] and Pine *et al.* [17] and review the theory which leads to a general expression for the temporal correlation function of multiply scattered light. In section 2.B, we discuss the calculation of the distribution of photon path lengths through the sample using the photon diffusion approximation and in section 2.C we discuss the method we use to calculate explicit expressions for the temporal autocorrelation functions we measure.

2.A. CORRELATION FUNCTION FOR MULTIPLY-SCATTERED LIGHT. — For simplicity, we consider a suspension of identical spherical particles randomly dispersed in a fluid and illuminated with laser light of wavelength λ . For specificity, we assume a slab geometry, as shown in figure 1a; other geometries will be discussed later. The suspension must be optically thick so that all the light entering the sample is scattered many times before exiting. Scattered light exiting the sample is collected from a small area near the sample surface (within approximately one mean free path, ℓ) and partially collimated so that roughly one coherence area is detected. The motion of the particles is probed by monitoring the time dependence of

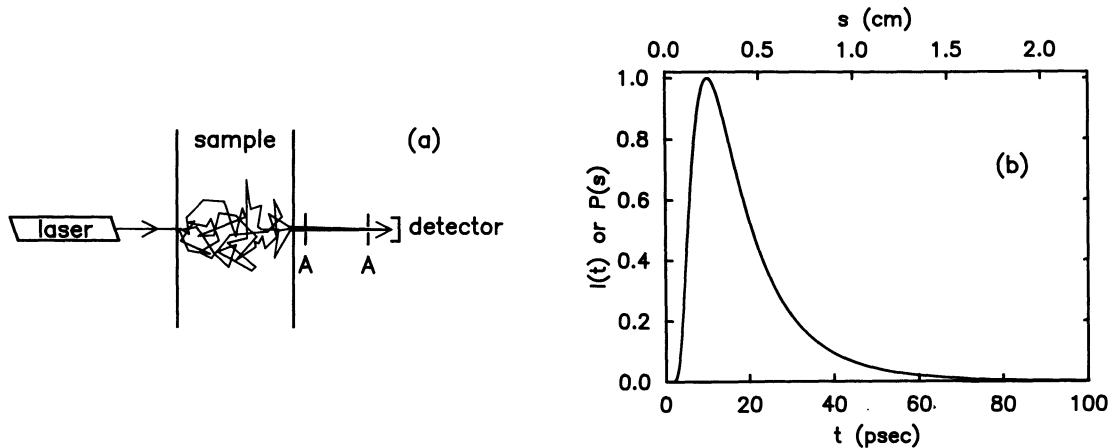


Fig. 1. — Transmission geometry for a point source. (a) A point source of light is incident on the sample on the left side and is collected from a point directly opposite the input point on the right side. Pinhole apertures (A) collimate the scattered light. (b) $I(t)$ vs t for transmission of a delta function pulse, $\delta(t)$, through a slab of thickness L . The plot can also be interpreted as $P(s)$ vs s since the fraction of photons travelling a distance s through the sample in a time $t = s/c$, where c is the velocity of light in the sample. Here, $L = 1$ mm, $\ell^* = 100$ μm , and $c = 2.25 \times 10^{10}$ cm/s (the speed of light in water). Note that $P(s)$ decays exponentially for large s .

the fluctuations of the scattered light. In DLS experiments, these fluctuations are usually characterized by the normalized temporal autocorrelation function,

$$g_1(\tau) = \frac{\langle E(0) E^*(\tau) \rangle}{\langle |E(0)|^2 \rangle}, \quad (2.2)$$

where $E(\tau)$ is the electric field of the scattered light collected by the detector and τ is the delay time. To calculate $g_1(\tau)$, we follow the approach of Maret and Wolf [4] and first consider a single light path through the sample. For a given sequence of scattering events at positions $\mathbf{r}_1, \dots, \mathbf{r}_n$ and with corresponding successive wavevector transfers $\mathbf{q}_i = \mathbf{k}_i - \mathbf{k}_{i-1}$, the product of the scattered electric field at time τ with that at time 0 will be

$$E^{(n)}(\tau) E^{(n)*}(0) = |E^{(n)}(0)|^2 \exp \left[i \sum_{i=1}^n \mathbf{q}_i \cdot \Delta \mathbf{r}_i(\tau) \right], \quad (2.3)$$

where $\Delta \mathbf{r}_i(\tau) = \mathbf{r}_i(\tau) - \mathbf{r}_i(0)$ is the distance the i -th particle moves in a time τ . The argument of the exponential,

$$\Delta \Phi^{(n)}(\tau) = \sum_{i=1}^n \mathbf{q}_i \cdot \Delta \mathbf{r}_i(\tau), \quad (2.4)$$

represents the aggregate phase shift of the scattered light due to the motion of all n scatterers in the time interval τ . Assuming that the fields belonging to different paths add incoherently, the average contribution to the normalized autocorrelation function of all paths of order n is

$$\langle E^{(n)}(\tau) E^{(n)*}(0) \rangle = I_0 P(n) \left\langle \prod_{i=1}^n e^{-i \mathbf{q}_i \cdot \Delta \mathbf{r}_i(\tau)} \right\rangle. \quad (2.5)$$

Here $P(n)$ is the fraction of the total scattered intensity, I_0 , in the n -th order paths and $\langle \rangle$ denotes averages over both the particle displacement, $\Delta \mathbf{r}(\tau)$, and the distribution of wavevectors \mathbf{q} . For large n , that is $n \gg n_0$, the transport of light through a sample is accurately described within the diffusion approximation. This allows $P(n)$ to be easily evaluated. Furthermore, the large number of scattering events in each path greatly simplifies the evaluation of the averages in equation (2.5).

For large n , we can relax the condition that the sum of the intermediate scattering vectors must equal the difference between the incident and exiting wavevectors, $\sum_i^n \mathbf{q}_i = \mathbf{k}_n - \mathbf{k}_0$. In addition, we also assume that successive scattering events are uncorrelated. Thus, the distribution of the \mathbf{q}_i is determined solely by the scattering form factor of a single sphere. Then, the right hand side of equation (2.5) becomes $P(n) \langle \exp[-i\mathbf{q} \cdot \Delta \mathbf{r}(\tau)] \rangle^n$. For Brownian motion, the distribution of $\Delta \mathbf{r}(\tau)$ is Gaussian and the average over particle motion is readily performed yielding

$$\langle E^{(n)}(\tau) E^{(n)*}(0) \rangle = I_0 P(n) \langle e^{-q^2 \langle \Delta r^2(\tau) \rangle / 6} \rangle_q^n, \quad (2.6)$$

where $\langle \rangle_q$ denotes the form-factor weighted average over q . For simple diffusion, $\langle \Delta r^2(\tau) \rangle = 6 D \tau$ where D is the diffusion coefficient of the particles.

The average over q can be performed explicitly for point-like scatterers which scatter light isotropically; this gives

$$\langle E^{(n)}(\tau) E^{(n)*}(0) \rangle = I_0 P(n) \left[\frac{\tau_0}{4 \tau} [1 - e^{-4 \tau / \tau_0}] \right]^n, \quad (2.7)$$

where $\tau_0 = (Dk_0^2)^{-1}$ and $k_0 = 2 \pi / \lambda$. However, for larger particles which scatter light anisotropically, the average over q is more difficult to perform. Thus, we restrict ourselves to small delay times, $\tau \ll \tau_0$, and retain only the first term in a cumulant expansion,

$$\langle e^{-Dq^2 \tau} \rangle_q^n \simeq \langle 1 - Dq^2 \tau \rangle_q^n = (1 - D \langle q^2 \rangle \tau)^n \simeq e^{-D \langle q^2 \rangle \tau n}. \quad (2.8)$$

We can compare this more general approximation with the exact expression, equation (2.7), for point-like scatterers by evaluating $\langle q^2 \rangle$ for a flat distribution,

$$\langle q^2 \rangle = \frac{\int q^2 d\Omega}{\int d\Omega} = \frac{\int q^2 q dq}{\int q dq} = 2 k_0^2, \quad (2.9)$$

where $d\Omega$ denotes the solid angle. This gives,

$$\langle E^{(n)}(\tau) E^{(n)*}(0) \rangle = I_0 P(n) e^{-(2 \tau / \tau_0) n}. \quad (2.10)$$

Expanding the exact expression in equation (2.7) gives

$$\langle E^{(n)}(\tau) E^{(n)*}(0) \rangle = I_0 P(n) e^{-2 n \tau / \tau_0 [1 - 1/3(\tau / \tau_0) + O(\tau / \tau_0)^3]}, \quad (2.11)$$

so that the cumulant expansion gives the correct results to leading order in τ / τ_0 . Furthermore, the effective decay time is $\tau_0 / 2n$, so that for large n , $\langle E^{(n)}(\tau) E^{(n)*}(0) \rangle$ decays essentially to zero before the higher order terms make a significant contribution.

Nevertheless, for large τ/τ_0 the cumulant expansion must fail since the exact expression in equation (2.7) decays as a power law, $(\tau/\tau_0)^{-n}$, due to the contributions of scattering at small q . We note, however, that at these long times low order scattering events dominate. For small n , the distribution of \mathbf{q}_i is not random but must satisfy the condition that $\sum_i \mathbf{q}_i = \mathbf{k}_n - \mathbf{k}_0$. This

will modify the average in equation (2.8) and could have the effect of at least partially offsetting the error introduced by the cumulate expansion.

Equation (2.8) can be readily generalized to treat the anisotropic scatterers typically used in experiments. Here, the single particle scattering intensity is peaked in the forward direction and $\langle q^2 \rangle$ is less than $2k_0^2$. Using the relation $\ell/\ell^* = \langle 1 - \cos \theta \rangle$, [10, 18] we have

$$\langle q^2 \rangle = \langle [2k_0 \sin(\theta/2)]^2 \rangle = 2k_0^2 \langle 1 - \cos \theta \rangle = 2k_0^2 \frac{\ell}{\ell^*}. \quad (2.12)$$

With this result and the cumulant expansion in equation (2.8), we can evaluate the average over q in equation (2.6) and obtain a simple expression for the contribution of the n -th order scattering paths to the autocorrelation function,

$$\langle E^{(n)}(\tau) E^{(n)*}(0) \rangle = I_0 P(n) e^{-(2\tau/\tau_0)(\ell/\ell^*)n}. \quad (2.13)$$

For isotropic scatterers, $\ell = \ell^*$, and we recover equation (2.10), the approximate result for point-like scatterers. We note that the accuracy of equation (2.13) improves as the scattering becomes more anisotropic. The second cumulant of $\langle e^{-Dq^2\tau} \rangle_q$ is $e^{-\frac{1}{2}(D\tau)^2[\langle q^4 \rangle - \langle q^2 \rangle^2]}$. For typical single-particle form factors, $F(q)$, we expect $\langle q^4 \rangle \sim \langle q^2 \rangle^2 \sim (\ell/\ell^*)^2$, so that the leading order correction to the cumulant expansion in equation (2.8) is $O[(\tau/\tau_0)(\ell/\ell^*)^2]$. Thus, for large scatterers, where $\ell^* \gg \ell$, the range of validity of equation (2.13) may extend up to $\tau \approx \tau_0$.

The total field autocorrelation function, $g_1(\tau)$, is obtained by summing over scattering paths of all orders

$$g_1(\tau) = \sum_{n=1}^{\infty} P(n) e^{-(2\tau/\tau_0)(\ell/\ell^*)n}. \quad (2.14)$$

If we rescale n by defining $n^* \equiv n/n_0 = (\ell/\ell^*)n$, the exponential term in this equation is identical to equation (2.10) for isotropic scatterers. Furthermore, for $n \gg n_0$, $P(n)$ can be written as a function of n^* rather than n . Physically, this reflects the fact that over length scales longer than ℓ^* , the scattering appears to be isotropic and the photon diffusion equation should be adequate to describe the transport of light. As a result, in this approximation,

$$g_1(\tau) = \sum_{n^*=1}^{\infty} P(n^*) e^{-(2\tau/\tau_0)n^*}. \quad (2.15)$$

This reflects a renormalization of the mean free path for anisotropic scatterers, so that the light may be viewed as undergoing an isotropic random walk with an average step length ℓ^* . We note that the decay rate of a given path depends critically on its length. Long paths reflect the aggregate contribution of many scattering events. Thus, each particle need move only a small distance for the total path length to change by a wavelength. This occurs in a short time, leading to a rapid decay rate. By contrast, short paths reflect the contribution of a small number of scattering events. Thus, each particle must undergo substantial motion for the total path length to change by a wavelength. This takes a longer time, leading to a slower decay.

The key to the solution of equation (2.15) is the determination of $P(n^*)$. This task is greatly simplified if we pass to the continuum limit. Thus, we approximate the sum over n^* by an integral over the path lengths, $s = n^* \ell^* (= n\ell)$, and obtain

$$g_1(\tau) = \int_0^\infty P(s) e^{-(2\tau/\tau_0)s/\ell^*} ds. \quad (2.16)$$

In this case, $P(s)$ is the fraction of photons which travel a path of length s through the scattering medium. Physically, equation (2.16) reflects the fact that a light path of length s corresponds to a random walk of s/ℓ^* steps and that $g_1(\tau)$ decays, on average, $\exp(-2\tau/\tau_0)$ per step. Now we can use the diffusion approximation to describe the random walk of the light, and $P(s)$ can be obtained from the solution of the diffusion equation for the appropriate experimental geometry. We emphasize, however, that the continuum approximation to the discrete scattering events will break down whenever there are significant contributions from short light paths.

2.B. BOUNDARY CONDITIONS AND CALCULATION OF $g_1(\tau)$ FROM $P(s)$. — Our method for determining $P(s)$ can be illustrated by considering a simple experiment. An instantaneous pulse of light is incident on the face of a sample which multiply scatters the light. The scattered photons will execute a random walk until they escape the sample. Here, we focus on those photons which exit the sample at some specified point, \mathbf{r}_d , on the boundary where they are detected. The flux of photons reaching \mathbf{r}_d is zero at $t = 0$, then increases to a maximum, and finally decreases back to zero at long times when all the photons have left the sample (see Fig. 1b). At time t , the photons arriving at point \mathbf{r}_d are those that have traveled a path length $s = ct$ through the sample. Thus, the flux of photons arriving at point \mathbf{r}_d at a given time is directly proportional to $P(s)$. The details of this time dependence, and hence the shape of $P(s)$, will depend on the experimental geometry.

To obtain $P(s)$ for a given experimental geometry we use the diffusion equation for light equation (2.1), to determine the dispersion induced in a delta function pulse as it traverses the scattering medium. We denote the density of diffusing photons within the medium by $U(\mathbf{r})$. For initial conditions, we exploit the fact that the direction of the incident light is randomized over a length scale comparable to ℓ^* and therefore take the source of diffusing light intensity to be an instantaneous pulse at a distance $z = z_0$ inside the illuminated face, where we expect that $z_0 \sim \ell^*$, that is

$$U(z, t = 0) = \delta(z - z_0, t). \quad (2.17)$$

In sections 3 and 4, where we calculate explicit expressions for the temporal autocorrelation functions for transmission and backscattering geometries, we discuss the consequences of approximating the source term with a delta function.

In addition to the initial conditions, the boundary conditions must ensure that there is no flux of *diffusing* photons entering the sample from the boundary. Thus, *outside* a sample consisting of a slab of thickness L between $z = 0$ and $z = L$,

$$\begin{aligned} J_+(z < 0) &= 0 \\ J_-(z > L) &= 0, \end{aligned} \quad (2.18)$$

where $J_+(z)$ and $J_-(z)$ are the fluxes of diffusing photons in the $+z$ and $-z$ directions, respectively. In the appendix we show that, within the diffusion approximation, the fluxes of diffusing photons *inside* the sample in the $\pm z$ directions are given by

$$J_\pm(z) = \frac{Uc}{4} \mp \frac{D\ell}{2} \frac{\partial U}{\partial z} \quad (2.19)$$

where J_{\pm} are taken to be always positive. The $Uc/4$ term will dominate the total flux in a given direction in the interior of the sample where the density of photons is high. However, the *net* flux in a given direction will be dominated by the gradient term, consistent with Fick's law

$$J = J_+ - J_- = -D_t \frac{\partial U}{\partial z}. \quad (2.20)$$

To obtain the boundary conditions, we consider the sample interface at $z = 0$ where $J_+ = 0$ and J_- is given by equation (2.19). Hence, $J(z = 0) = -J_-(0)$ and the net flux is directed out of the sample. Inside the sample, a distance ℓ^* away from the boundary, the total flux is given by equation (2.20). Since ℓ^* is the minimum distance over which the intensity can change within the diffusion approximation, these two expressions for the flux near the boundary must be equal :

$$-J_-(0) = -\left(\frac{Uc}{4} + \frac{D\ell}{2} \frac{\partial U}{\partial z}\right)\Big|_{z=0} = J(0) = -D_t \frac{\partial U}{\partial z}\Big|_{z=0}. \quad (2.21)$$

Simplifying this expression, we obtain the boundary condition,

$$\left(U - \frac{2}{3}\ell^* \frac{\partial U}{\partial z}\right)\Big|_{z=0} = 0. \quad (2.22)$$

Alternatively, this boundary condition can be obtained directly by setting the expression for J_+ in equation (2.19) equal to zero [19]. Similar procedures can be used to derive a boundary condition at $z = L$. In general, the boundary conditions at either interface are given by

$$\left(U + \frac{2}{3}\ell^* \hat{n} \cdot \nabla U\right)\Big|_{z=0,L} = 0, \quad (2.23)$$

where \hat{n} is the outward normal [10]. We emphasize the approximate nature of these boundary conditions which were obtained by requiring that the *net* inward flux of diffusing photons be zero [20]. More generally, the flux must be zero for all incoming directions. However, this more stringent condition can only be met by going beyond the diffusion approximation to a more general transport theory [10, 21].

Using the boundary conditions in equation (2.23), we can solve the diffusion equation for $U(\mathbf{r}, t)$ for a given experimental geometry [22] and then calculate the time-dependent flux of light emerging from the sample at time t from equation (2.19) evaluated at the exit point. All light emerging from the sample at time t has traveled a distance $s = ct$. Thus, the fraction of light, $P(s)$, which travels a distance s through the sample is simply proportional to the flux of light emerging from the sample at time $t = s/c$:

$$P(s) \propto J_{\text{out}}(\mathbf{r}, t)\Big|_{\mathbf{r}_d} = \left(\frac{Uc}{4} - \frac{c\ell}{6} \hat{n} \cdot \nabla U\right)\Big|_{\mathbf{r}_d} = \frac{Uc}{2}\Big|_{\mathbf{r}_d} \quad (2.24)$$

where \mathbf{r}_d denotes the exit point of the light and, again, \hat{n} is the *outward* normal. The last equality in equation (2.24) follows from the boundary condition, equation (2.23). Having determined $P(s)$ for a given geometry, equation (2.16) can be used to calculate $g_1(\tau)$.

2.C. DIRECT CALCULATION OF $g_1(\tau)$. — The calculation of $g_1(\tau)$ can be greatly simplified by noting that equation (2.16) is essentially the Laplace transform of $P(s)$. Thus, instead of solving the diffusion equation to obtain $P(s)$, we can solve the Laplace transform of the

diffusion equation and obtain $g_1(\tau)$ directly. To this end, we introduce a simple change of variables in equation (2.1) and let $t = s/c$. Recalling that $D_\ell = c\ell^*/3$, equation (2.1) becomes,

$$\nabla^2 U - \frac{3}{\ell^*} \frac{\partial U}{\partial s} = 0. \quad (2.25)$$

Multiplying both sides by $\exp(-ps)$ and integrating with respect to s from 0 to ∞ , we obtain the Laplace transform of the diffusion equation,

$$\nabla^2 \bar{U} - \frac{3p}{\ell^*} \bar{U} = -\frac{3}{\ell^*} U_0(\mathbf{r}) \quad (2.26)$$

where $\bar{U} = \bar{U}(\mathbf{r}, p)$ is the Laplace transform of $U(\mathbf{r}, s)$,

$$\bar{U}(\mathbf{r}, p) = \int_0^\infty e^{-ps} U(\mathbf{r}, s) ds, \quad (2.27)$$

and $U_0(\mathbf{r}) = \lim_{t \rightarrow 0} U_0(\mathbf{r}, t) = \delta(z - z_0, t)$ [22]. Equation (2.26) can be solved subject to the

Laplace transform of the same boundary conditions used previously equation (2.23), using Green's function techniques. This method is carefully discussed by Carslaw and Jaeger [22] where explicit solutions to the diffusion equation and its Laplace transform are given for most geometries of experimental interest. The solution to equation (2.26) can be related directly to $g_1(\tau)$ by taking the Laplace transform of $P(s)$ and using equation (2.24) to write

$$\bar{P}(p) = \int_0^\infty P(s) e^{-ps} ds \propto \frac{c}{2} \bar{U}(\mathbf{r}, p) \Big|_{\mathbf{r}_d}. \quad (2.28)$$

Comparing equations (2.16) and (2.28), we see that

$$g_1(\tau) = \frac{\bar{U}(\mathbf{r}, p) \Big|_{\mathbf{r}_d}}{\bar{U}(\mathbf{r}, 0) \Big|_{\mathbf{r}_d}} \quad (2.29)$$

where we have made the identification, $p = (2\tau/\tau_0)/\ell^*$, and $\bar{U}(\mathbf{r}, p)$ has been normalized so that $g_1(0) = 1$. Thus, by solving the Laplace transform of the diffusion equation we can obtain the desired autocorrelation function directly. We illustrate this method of solution in sections 3 and 4 with explicit examples for transmission and backscattering geometries.

Finally, for comparison to our experiments, we note that we usually measure normalized intensity autocorrelation functions, $\langle I(\tau) I(0) \rangle / \langle I(0) \rangle^2 = 1 + \beta g_2(\tau)$, where β is determined primarily by the collection optics and is defined so that $g_2(0) = 1$. For most systems of experimental interest, the scattered electric field is a complex Gaussian random variable and the intensity autocorrelation function is related to the field autocorrelation function calculated above by the Siegert relation,

$$g_2(\tau) = |g_1(\tau)|^2. \quad (2.30)$$

Wolf *et al.* [18] have experimentally verified that there is no observable deviation from Gaussian statistics for strong multiple scattering in samples similar to ours. In addition, by measuring $g_1(\tau)$ directly in heterodyne experiments, we have verified the validity of equation (2.30) for the correlation functions reported here.

3. Transmission.

The first experimental geometry we consider is transmission through a slab of thickness L and infinite extent [6, 15]. The light is incident on one side of the slab, and is detected after it has diffused a distance L across the sample. The incident light beam can either be focused to a point on the face, as illustrated in figure 1a, or expanded to uniformly fill the face of the slab, as illustrated in figure 2. The autocorrelation functions for these two experimental geometries are different and can be calculated by solving the Laplace transform of the diffusion equation as previously discussed. In both cases, we take the source of diffusing intensity to be a distance $z = z_0$ inside the illuminated face where we expect that $z_0 \sim \ell^*$.

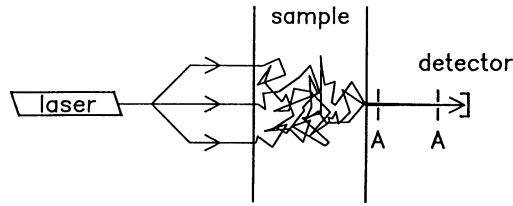


Fig. 2. — Transmission geometry for an extended source. An extended source of light (plane wave) is incident on the sample on the left side and is collected from a point directly opposite the center of the input beam on the right side. A — pinhole apertures.

We first consider the case of uniform illumination of one side by an extended source so that $U(x, y, z, t) = \delta(z - z_0, t)$. The solution of the diffusion equation using the Laplace transform is given in Carslaw and Jaeger [22] (§ 14.3) for this geometry and for these boundary and initial conditions. They obtain

$$\bar{U} = \frac{1}{2 D_\ell \alpha} e^{-\alpha |z - z_0|} + A \sinh \alpha z + B \cosh \alpha z, \quad (3.1)$$

where $\alpha^2 \equiv 3 p / \ell^* = 6 \tau / \tau_0 \ell^{*2}$ and $D_\ell = c \ell^* / 3$. The coefficients A and B are chosen so that the boundary conditions, equation (2.23), are satisfied at $z = 0$ and $z = L$. After tedious, but straightforward algebra, we obtain

$$g_1(\tau) = \frac{\frac{L + (4/3) \ell^*}{z_0 + (2/3) \ell^*} \left\{ \sinh \left[\frac{z_0}{\ell^*} \sqrt{\frac{6 \tau}{\tau_0}} \right] + \frac{2}{3} \sqrt{\frac{6 \tau}{\tau_0}} \cosh \left[\frac{z_0}{\ell^*} \sqrt{\frac{6 \tau}{\tau_0}} \right] \right\}}{\left(1 + \frac{8 \tau}{3 \tau_0} \right) \sinh \left[\frac{L}{\ell^*} \sqrt{\frac{6 \tau}{\tau_0}} \right] + \frac{4}{3} \sqrt{\frac{6 \tau}{\tau_0}} \cosh \left[\frac{L}{\ell^*} \sqrt{\frac{6 \tau}{\tau_0}} \right]} \quad (3.2a)$$

$$\approx \frac{\left(\frac{L}{\ell^*} + \frac{4}{3} \right) \sqrt{\frac{6 \tau}{\tau_0}}}{\left(1 + \frac{8 \tau}{3 \tau_0} \right) \sinh \left[\frac{L}{\ell^*} \sqrt{\frac{6 \tau}{\tau_0}} \right] + \frac{4}{3} \sqrt{\frac{6 \tau}{\tau_0}} \cosh \left[\frac{L}{\ell^*} \sqrt{\frac{6 \tau}{\tau_0}} \right]}, \quad (3.2b)$$

where the second expression holds for $\tau \ll \tau_0$. The characteristic time scale in these expressions is $\tau_0 (\ell^* / L)^2$.

For the second geometry, we consider light incident from a point source on axis with the detector so that $U(x, y, x, t) = \delta(x, y, z - z_0, t)$. The solution for this geometry and these boundary and initial conditions can again be found in Carslaw and Jaeger [22] (§ 14.10) :

$$\bar{U} = \frac{1}{4\pi D_\ell} \int_0^\infty \frac{\xi J(\xi R)}{\eta} [e^{-\eta|z-z_0|} + A \sinh \eta z + B \cosh \eta(L-z)] d\xi \quad (3.3)$$

where $\eta = \sqrt{\xi^2 + \alpha^2}$, $\alpha^2 \equiv 3p/\ell^* = 6\tau/\tau_0 \ell^{*2}$, and $R = 0$ when the source is on axis with the detector. The coefficients A and B are again found by applying the boundary conditions. We obtain,

$$g_1(\tau) \propto \int_{(L/\ell^*)\sqrt{6\tau/\tau_0}}^\infty [A(s) \sinh s + e^{-s(1-z_0/L)}] ds \quad (3.4a)$$

where

$$A(s) = \frac{(\varepsilon s - 1) [\varepsilon s e^{-sz_0/L} + (\sinh s + \varepsilon s \cosh s) e^{-s(1-z_0/L)}]}{(\sinh s + \varepsilon s \cosh s)^2 - (\varepsilon s)^2} \quad (3.4b)$$

and $\varepsilon = 2\ell^*/3L$. Again, the characteristic time scale for the decay of the autocorrelation function in equation (3.4) is $\tau_0(\ell^*/L)^2$. This time scale reflects the diffusive nature of the transport of the light, which introduces a characteristic path length, $s_c = n_c \ell = n_c^* \ell^*$, where $n_c^* = (L/\ell^*)^2$ is the mean number of steps for a random walk of end-to-end distance L and average step length ℓ^* . Physically, this characteristic time scale corresponds to the time taken for the characteristic path length to change by $\sim \lambda$, so that the total phase shift is roughly unity. Thus, we can estimate the typical distance an individual particle has moved from $n_c \langle q^2 \rangle \langle \Delta r^2 \rangle \approx 1$, which gives $\Delta r_{rms} \approx \lambda \ell^*/2\pi L$. Since $\ell^*/L \ll 1$, the typical length scale over which particle motion is probed by DWS in transmission is much smaller than the wavelength. This reflects the fact that the decay of the autocorrelation function is due to the cumulative effect of many scattering events, so that the contribution of individual particles to the total decay is small. *This is in striking contrast to ordinary dynamic light scattering where, by varying q , length scales greater than or roughly equal to the wavelength are probed.* Similarly, the time scale over which particle motion is probed with DWS is much shorter than with DLS. Thus, by adjusting the sample thickness L in transmission measurements, DWS provides a means for varying the range of length and time scales over which particle motion can be measured using dynamic light scattering techniques.

Another significant difference between DLS and DWS is the dependence on scattering angle. In DLS, varying the angle changes the scattering vector, q , thus varying the length scale over which motion is probed. By contrast, in DWS, the diffusive nature of the transport ensures that the transmitted light has no appreciable dependence on angle and we do indeed find that the measured autocorrelation functions are independent of detection angle in transmission.

Autocorrelation functions measured in transmission are shown in figure 3. The sample consisted of an aqueous suspension of 0.605- μm -diam. polystyrene latex spheres at a volume fraction of $\phi = 0.012$ in a 1.0 mm thick cuvette. There is no unscattered light transmitted through the sample, insuring that the strong multiple scattering limit is achieved. The data in the lower curve were obtained when the sample was illuminated uniformly by a 1-cm diameter beam from an argon ion laser with $\lambda_0 = 488 \text{ nm}$. Imaging optics collected the transmitted light from a 50 μm spot on the opposite side of the sample from a point near the center of the illuminated area. For comparison, the upper curve shows data obtained when the incident

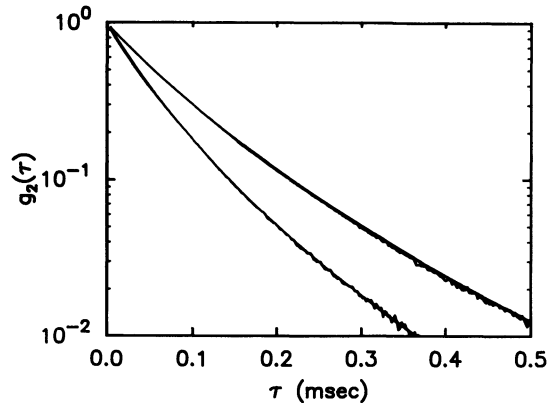


Fig. 3. — Intensity autocorrelation functions vs time for transmission through 1-mm thick cells with 0.605- μm -diameter polystyrene spheres and $\phi = 0.012$. The upper curve is for a point source (see Fig. 1a) and the lower curve is for an extended plane wave source (see Fig. 2). Smooth lines are fits to the data by equations (3.2) and (3.4) with $\ell^* = 167 \mu\text{m}$ for the extended source and $\ell^* = 166 \mu\text{m}$ for the point source.

beam was focused to a point on one side of the sample and transmitted light was collected from a point on axis with the incident spot. These data clearly decay more slowly than the data obtained with an extended source illumination. Physically, this difference reflects the fact that for the extended source there is a larger contribution from long paths, resulting in a faster decay than for the point source.

To compare these data to the expression for the autocorrelation function derived above, we take $z_0 = (4/3) \ell^*$, but note that the solutions are insensitive to the exact value used since, in general, $z_0 \sim \ell^*$ and $\ell^*/L \ll 1$. The value chosen for z_0 affects only the first few steps of a random walk which typically consists of a great number of steps. Thus, the relative contribution of the first few steps is small. In figure 3, the solid lines through the data are fits to the appropriate equations above. The time constant $\tau_0 \equiv (Dk_0^2)^{-1}$ is set equal to 4.52 ms where D was obtained from a DLS measurement in the single scattering limit using $\phi = 10^{-5}$. The diffusion coefficient D remains independent of concentration for the particle concentrations used in these measurements. For both cases, excellent agreement is found between the data and the predicted forms of $g_2(\tau)$. The only fitting parameter is ℓ^* and values of $\ell^* = 167 \mu\text{m}$ for the extended source and $\ell^* = 166 \mu\text{m}$ for the point source are obtained. This excellent consistency for the fitted values of ℓ^* confirms that the different decay rates in figure 3 are due solely to geometric effects. The values obtained from the fit to the data are in reasonable agreement with Mie scattering theory, $\ell^* = 180 \mu\text{m}$. Nevertheless, there is a discrepancy of about 7 %, with the measured values lower than predicted. This is not experimental error, as a similar discrepancy is found for other polystyrene latex samples with different sizes and different volume fractions. The values obtained from DWS measurements in transmission are consistently lower than the predicted values, typically by about 10 %. This discrepancy is probably not due to the consequences of particle correlation on the value of ℓ^* . The particle interactions in these polystyrene samples can be approximated as hard sphere repulsion, allowing the particle correlations to be determined [4]. These are relatively weak for $\phi < 0.1$, leading to negligible effect on ℓ^* . Instead, we believe that the discrepancy arises from the approximate nature of the boundary condition that we use, equation (2.23). In particular, we neglect the possibility of any reflection of the light due to the discontinuity of the average index of refraction at the boundary. Including this effect will modify the boundary

condition and will result in a renormalization of the value of ℓ^* obtained from DWS transmission measurements. If this effect is not included, the apparent ℓ^* measured will be less than the correct value.

While the autocorrelation functions shown in figure 3 are clearly not single exponentials, their curvature in the semi-logarithmic plot is not large. This reflects the existence of a dominant characteristic path length and time scale for these data, as expected. This also suggests the suitability of analyzing the data by means of the first cumulant Γ_1 , or the logarithmic derivative at zero time delay. For equation (3.2), the first cumulant is given by

$$\Gamma_1 = \left. \frac{\partial \ln g_1(\tau)}{\partial \tau} \right|_{\tau=0} \approx \frac{(L/\ell^*)^2 + 4(L/\ell^*) + 8/3}{\tau_0(1 + 4\ell^*/3L)}. \quad (3.5)$$

For equation (3.4), the first cumulant must be evaluated numerically. Measurements of $\sqrt{\Gamma_1}$ as a function of sample thickness are shown in figure 4 for several volume fractions. These data were obtained using polystyrene latex spheres with a diameter of 0.497 μm . The incident beam was focused onto the face of a wedge-shaped cell, allowing the thickness to be varied by translating the cell in the beam. The angle of the wedge was about 3° , so the cell shape had very little effect on the form of the autocorrelation function. The data in figure 4 show the expected linear dependence of $\sqrt{\Gamma_1}$ over a broad range of concentrations confirming the diffusive nature of the transport of light. It is apparent that the data do not extrapolate through the origin but that the L -intercepts are a monotonically decreasing function of particle concentration and consistent with equation (3.5), to within experimental uncertainty. The different slopes are due primarily to the concentration dependence of ℓ^* , which is expected to scale inversely with particle density for the volume fractions used here.

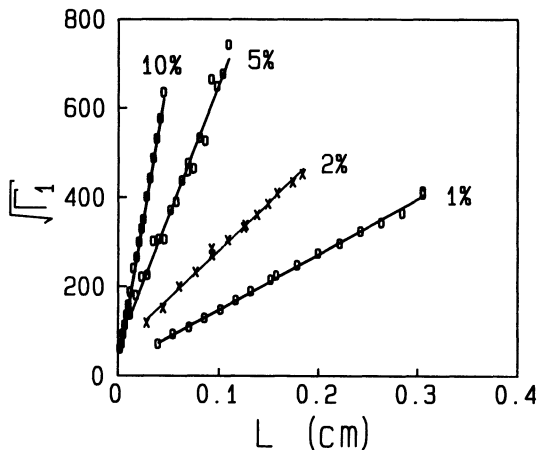


Fig. 4. — Square root of the first cumulant Γ_1 of the intensity autocorrelation function vs sample thickness L . The data were obtained using the point-source transmission geometry for 0.497- μm -diameter spheres with volume fractions of 1 %, 2 %, 5 %, and 10 %. The linear dependence shown in the plot confirms the diffusive nature of the transport of light.

4. Backscattering.

The second geometry we consider is that of backscattering [4, 5, 6, 15]. Here, the light is incident uniformly on one face of a slab of thickness, L , and the scattered light is collected

from the same face, as illustrated in figure 5a. In deriving a functional form for the autocorrelation function, we would like to maintain the simplicity and elegance of the Laplace transform approach used in the case of transmission. However, we must be extremely cautious in using this approach for backscattering. In obtaining the Laplace transform in equation (2.16), we have used a continuum approximation to change the summation over paths in equation (2.15) to an integral. However, since $s = n\ell$ and we must have at least one scattering event, we require $n \geq 1$; thus, the lower bound on s must be ℓ rather than 0. Equivalently, for isotropic scatterers, where $\ell = \ell^*$, the decay time for a path of length s is $\exp[-(2\tau/\tau_0)s/\ell]$. Allowing $s < \ell$ leads to unphysically long decay times, since $\tau_0/4$ represents the shortest decay time possible, corresponding to light singly scattered through 180° . Similarly, for anisotropic scatterers, where $\ell^* > \ell$, we require $s \geq \ell^*$ to obtain physically meaningful decay times. However, in order to maintain the simplicity of the Laplace transform, the lower bound on the integral must be zero. For transmission, this does not present a problem since the shortest possible paths are $s = L$, so that $n \gg 1$. By contrast, for backscattering, short paths do contribute and thus, in using the diffusion approximation, we must ensure that the contribution of the unphysically short paths is suppressed.

A simple way of achieving this is to solve the diffusion equation using an initial condition of a source at a fixed distance, z_0 , in from the illuminated face at $z = 0$. This ensures that there are no contributions from paths shorter than z_0 . Physically we can regard this as the source of the diffusing intensity, which we expect to be peaked at $z_0 \sim \ell^*$. Thus, for the initial condition we take $U(\mathbf{r}, t = 0) = \delta(x, y, z - z_0, t)$ and for the boundary conditions again we use equation (2.23). The solution for this geometry is the same as for the case of transmission with an extended source, but here we evaluate it at the incident face and obtain,

$$G_1(\tau) = \frac{\sinh \left[\sqrt{\frac{6\tau}{\tau_0}} \left(\frac{L}{\ell^*} - \frac{z_0}{\ell^*} \right) \right] + \frac{2}{3} \sqrt{\frac{6\tau}{\tau_0}} \cosh \left\{ \sqrt{\frac{6\tau}{\tau_0}} \left(\frac{L}{\ell^*} - \frac{z_0}{\ell^*} \right) \right\}}{\left(1 + \frac{8}{3} \frac{\tau}{\tau_0} \right) \sinh \left[\frac{L}{\ell^*} \sqrt{\frac{6\tau}{\tau_0}} \right] + \frac{4}{3} \sqrt{\frac{6\tau}{\tau_0}} \cosh \left[\frac{L}{\ell^*} \sqrt{\frac{6\tau}{\tau_0}} \right]}. \quad (4.1)$$

For a sample of infinite thickness, equation (4.1) simplifies,

$$G_1(\tau) = \frac{e^{-(z_0/\ell^*) \sqrt{6\tau/\tau_0}}}{1 + \frac{2}{3} \sqrt{\frac{6\tau}{\tau_0}}}. \quad (4.2)$$

We note that the initial condition of a source at z_0 appears explicitly in the solution, reflecting the importance of the contribution of the short paths. In fact, we expect there to be a distribution in the position of the apparent source, z_0 . Thus we must integrate equation (4.2) over a distribution of sources, $f(z_0)$. While the exact form of $f(z_0)$ is unknown, we do know that $f(z_0)$ goes to zero as $z_0 \ll \ell^*$ and for $z_0 \gg \ell^*$. Furthermore, we expect $f(z_0)$ to be peaked near $z_0 \sim \ell^*$. Thus, to leading order in $\sqrt{\tau/\tau_0}$, $g_1(\tau)$ is given by equation (4.2), with z_0/ℓ^* replaced by $\langle z_0 \rangle / \ell^*$, the average over the source distribution $f(z_0)$. The first order correction is $[\langle z_0^2 \rangle / \langle z_0 \rangle^2 - 1] \tau / \tau_0$, which is small for a narrow distribution $f(z_0)$. Physically, we can think of $\langle z_0 \rangle$ as the average position of the source of diffusing intensity, and we expect that the exact form of the distribution $f(z_0)$, and therefore $\langle z_0 \rangle$, will depend on the anisotropy of the scattering as reflected by ℓ^*/ℓ .

In contrast to transmission, in backscattering there is no well-defined characteristic path length set by the sample thickness. In fact, since paths of all lengths contribute in backscattering, the autocorrelation function consists of contributions from all orders of

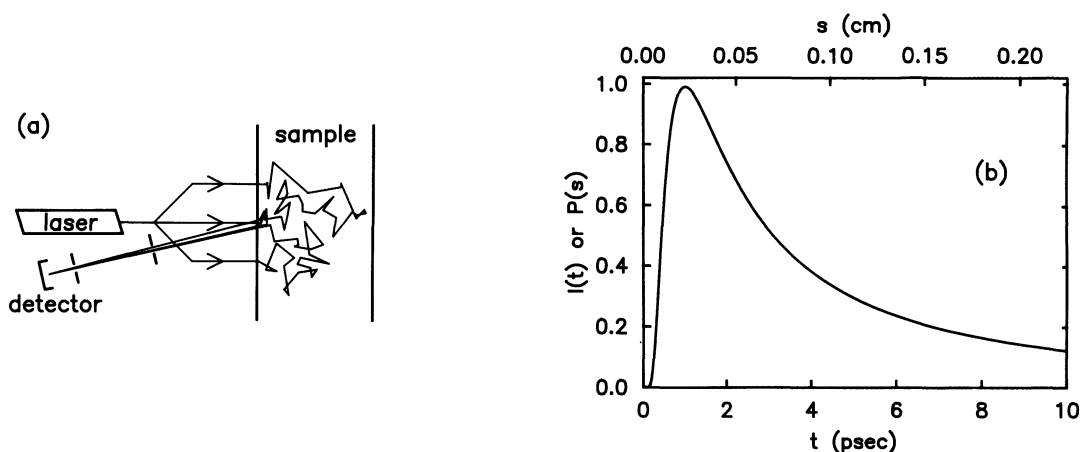


Fig. 5. — Backscattering geometry for an extended source. (a) An extended plane wave source of light is incident on the sample from the left side and is collected from a point near the center of the illuminated area. (b) $I(t)$ vs t for backscattering of a delta function pulse, $\delta(t)$, from a semi-infinite slab of thickness L . The plot can also be interpreted as $P(s)$ vs s since the fraction of photons travelling a distance s through the sample in a time $t = s/c$, where c is the velocity of light in the sample. Here, $L = 1$ mm, $\ell^* = 100$ μm , and $c = 2.25 \times 10^{10}$ cm/s (the speed of light in water). Note that $P(s)$ decays as $s^{-3/2}$ for large s .

multiple scattering. As a consequence, there is a much broader distribution of time scales in the decay. The longer paths consist of a larger number of scattering events and thus decay more rapidly, probing the motion of individual particles over shorter length and time scales. By contrast, the shorter paths consist of a smaller number of scattering events thus decaying more slowly and probing the motion of individual particles over longer length and time scales. This feature is particularly advantageous for exploring the dynamics of interacting systems, which can have a broad distribution of relaxation rates associated with motion over different lengths scales.

An autocorrelation function measured in backscattering is shown in figure 6. The sample consisted of an aqueous suspension of 0.412- μm -diam. polystyrene latex spheres at a volume fraction of $\phi = 0.05$ in a 5 mm thick cuvette. It was illuminated by a uniform beam, 1 cm in diameter; light from a 50 μm diameter spot near the center of the illuminated area was imaged onto the detector. The scattering angle was $\sim 175^\circ$, although we found virtually no dependence of the results on scattering angle when it was varied $\sim 20^\circ$ from that used here, as expected for diffusing light. After subtracting the baseline, the logarithm of the normalized autocorrelation function, is plotted as a function of time, in figure 6a. The large amount of curvature exhibited by the data reflects the contributions of paths with a wide range of length scales, leading to a wide range of decay times. As suggested by equation (4.2), the expression for $g_1(\tau)$ for DWS in backscattering, we replot the data in figure 6b as a function of the square root of time, in units of τ_0 . We use $\tau_0 = 3.01$ ms, as measured experimentally in the single scattering limit, and consistent with the value calculated from the Stokes-Einstein relation. The solid line is a fit to the functional form given by equation (4.2), and is in reasonably good agreement with the data. However, to within the precision of experiment, the data shown in figure 6 is linear over nearly three decades of decay when plotted logarithmically as a function of the square root of time. This suggests that the data can be more simply described using

$$G_1(\tau) = e^{-\gamma \sqrt{6\tau/\tau_0}} \quad (4.3)$$

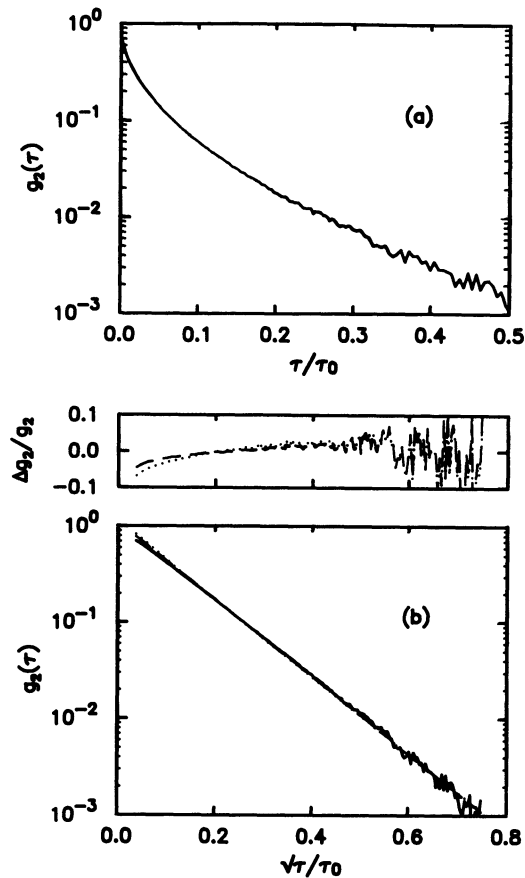


Fig. 6. — Intensity autocorrelation function for backscattering from a 5-mm thick cell containing 0.412- μm -diameter polystyrene spheres with $\phi = 0.05$. (a) Data is plotted as a function of reduced time. A large degree of curvature is evident. (b) Data is plotted as a function of the square root of reduced time. The dotted line through the data is a fit to the more exact form in equation (4.2). The dashed line through the data is a fit to the simpler form of equation (4.3). The residuals are shown above as a function of the square root of the reduced time. The simpler exponential decay with square root of time provides an excellent description of the data.

where $\gamma = \langle z_0 \rangle / \ell^* + 2/3$. This result was obtained previously using the simpler, but less rigorous, boundary condition, $U(z = 0) = 0$ [6, 23].

The behavior of the autocorrelation function shown in figure 6 is in fact quite general. For particles with diameters comparable to or greater than λ , where $\ell^*/\ell \gg 1$, the simple exponential form given in equation (4.3) is observed. For small particles, where $\ell^*/\ell \approx 1$, there is some curvature for data plotted logarithmically vs square root of time. The data curves upward or downward, depending on whether polarized or depolarized light is detected [24]. However, the theory we develop, expressed in equation (4.2), always exhibits a subtle upward curvature when plotted logarithmically vs square root of time. MacKintosh and John have obtained similar results using diagrammatic techniques [16]. Therefore, since the curvature in the data is generally small and may either be up or down, it is most convenient to use the very simple form in equation (4.3) to describe the shape of the autocorrelation function.

The slope of the autocorrelation function, when plotted in this fashion, is determined solely by τ_0 and γ . To obtain better agreement between theory and experiment, it is essential to properly account for the contributions of the short paths. This can be done by ensuring that the difference between initial and final wavevectors is strictly $2k_0$, as required for backscattering, and by limiting the momentum transfer in any single scattering event to properly reflect the form factor of the scatterers. By contrast, if this is not done, the contributions of the short paths are over estimated in the diagrammatic approach, leading to a prediction [15] for the autocorrelation function that describes the initial decay reasonably well, but fails at longer times by predicting a power-law decay, in sharp disagreement with the data.

The value of γ reflects the relative contribution of short paths to the backscattered light. These paths involve few scattering events and hence decay more slowly. A larger contribution of short paths leads to a slower total decay of the autocorrelation function, and a smaller value of γ . Using samples of known τ_0 , we find experimentally that γ depends on both polarization and on the anisotropy of the scattering, as characterized by ℓ^*/ℓ . The dependence of γ on polarization is strongest for isotropic scatterers, when $\ell^*/\ell \rightarrow 1$, as illustrated by the data shown in figure 7. These data are obtained from a $\phi = 0.02$ sample of $0.091 \mu\text{m}$ -diameter spheres, for which $\ell^*/\ell \approx 1.1$. The sample is illuminated by linearly polarized light, and an analyzer is used to detect scattered light whose polarization is either parallel or perpendicular to the incident light. The autocorrelation function for the perpendicular polarization decays more rapidly, because the analyzer discriminates against the low order paths which retain a high degree of their incident polarization. This reflects the contribution of multiple scattering paths for which the diffusion approximation is more appropriate. The value measured is $\gamma = 2.5$. By contrast, the autocorrelation function for the parallel polarization decays more slowly, because of the additional contribution of the low order scattering paths which have a longer decay time. We note, however, that the form of the autocorrelation function is still the same, remaining nearly linear when plotted exponentially as a function of the square root of time. Here, the value measured is $\gamma = 1.6$. By contrast, for very anisotropic scatterers, the dependence of γ on polarization is very weak. This is also illustrated in figure 7 which shows data obtained using a $\phi = 0.02$ sample of $0.605 \mu\text{m}$ diameter spheres, for which $\ell^*/\ell \approx 10$. The autocorrelation function for the perpendicular polarization again decays

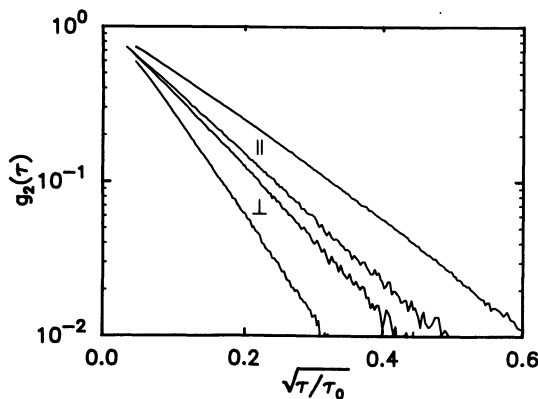


Fig. 7. — Intensity autocorrelation functions vs square root of reduced time for backscattering for parallel and perpendicular polarizations. The uppermost and lowermost curves are for $0.091\text{-}\mu\text{m}$ -diameter spheres, with $\gamma_{\parallel} = 1.6$ and $\gamma_{\perp} = 2.9$ ($\ell^*/\ell = 9.74$). The two middle curves are for $0.605\text{-}\mu\text{m}$ -diameter spheres with $\gamma_{\parallel} = 2.0$ and $\gamma_{\perp} = 2.1$ ($\ell^*/\ell = 1.12$).

faster, with $\gamma_{\perp} = 2.1$, but the difference for the parallel polarization is much smaller, with $\gamma_{\parallel} = 2.0$.

We summarize the dependence of γ on ℓ^*/ℓ for both polarizations in figure 8. The data are obtained by varying the size of the spheres to vary ℓ^*/ℓ , since for the particle sizes used here this ratio is nearly a monotonic function of sphere diameter. In all cases, $\phi = 0.02$. The data suggest that, for each polarization, γ asymptotically approaches a constant as ℓ^*/ℓ becomes large. Physically, this reflects the diminishing contributions of the short paths as the scattering becomes more strongly peaked in the forward direction. In this case, the diffusion approximation, which is scalar in nature, should apply. Therefore, $g_1(\tau)$ becomes a function of τ/τ_0 only, and thus, in this limit, γ does not depend strongly on ℓ^*/ℓ . In fact, an asymptotic value of $\gamma = 2.1$ is predicted theoretically by properly considering the contribution of the short paths to the autocorrelation function at long times [16]. Furthermore, the trends observed in figure 8 for the dependence of γ on both ℓ^*/ℓ and polarization are reasonably consistent with the predictions made using diagrammatic techniques.

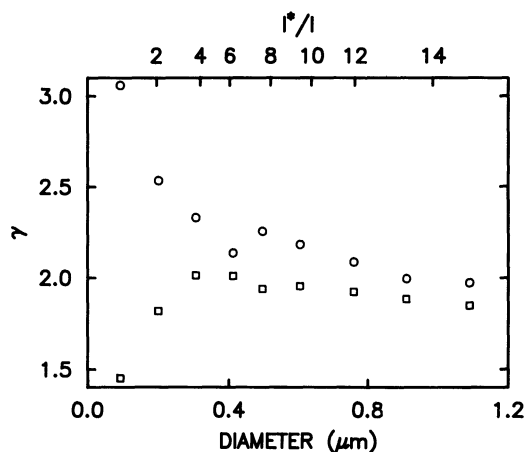


Fig. 8. — Experimental values of γ vs particle diameter and ℓ^*/ℓ for parallel (squares) and perpendicular polarizations (circles).

5. Absorption.

In any physical system there will always be absorption of light, either by the scatterers themselves or by the solvent in which they are suspended. Furthermore, the effects of absorption will be enhanced in the multiple scattering limit because the path lengths of the light and the number of scattering events are greatly increased. However, the consequences of absorption for the autocorrelation function can be readily determined. For any scattering geometry, $P(s)$ is the fraction of the scattered intensity associated with paths of length $s = n\ell$. With absorption by either the solvent or the scatterers, the intensity of light travelling a path of length s is attenuated exponentially by a factor $\exp(-s/\ell_a)$, where ℓ_a is the absorption length. Thus, we write $P'(s) = P(s) \exp(-s/\ell_a)$, where $P(s)$ is determined solely by geometry, as before. Then equation (2.16) has the form :

$$G_1(\tau) = I_0 \int P(s) e^{-s/\ell_a - (2\tau/\tau_0)s/\ell^* ds} . \quad (5.1)$$

Since both terms in the exponent are linear in s , the effect of the absorption is mathematically the same as shifting the time scale. Thus all of our previous analysis for different geometries is directly applicable if we simply make the substitution :

$$\tau/\tau_0 \rightarrow \ell^*/2\ell_a + \tau/\tau_0. \quad (5.2)$$

For example, in backscattering the form of the autocorrelation function for equation (4.3) becomes

$$g_1(\tau) = \exp \left(-\gamma \sqrt{\frac{6\tau}{\tau_0} + \frac{3\ell^*}{\ell_a}} \right). \quad (5.3)$$

Thus, absorption will significantly affect the decay of the autocorrelation function only for time scales less than $(\ell^*/2\ell_a)\tau_0$. For polystyrene spheres in water, $\ell_a > 100$ cm at optical wavelengths ; thus, for 0.497- μ m-diam. spheres at a volume fraction $\phi = 0.1$, $(\ell^*/2\ell_a)\tau_0 < 0.3$ μ s which is much shorter than the time scales of our measurements.

In order to observe the effects of absorption, we dissolve varying amounts of methyl red, an absorbing dye, in a suspension of 0.497- μ m diameter polystyrene spheres with $\phi = 0.01$, and measure the autocorrelation function in backscattering. The results are shown in figure 9. The absorption lengths are $\ell_a = 4.87$ mm for the upper curve and $\ell_a = 2.53$ mm for the lower curve. Physically, the effect of the absorption is to reduce the contribution of the longer paths to the decay of the autocorrelation function. These paths would otherwise contribute a rapid, initial decay of the correlation function. This effect is clearly evident in figure 9 by the rounding of the correlation function at early times.

A comparison of the prediction of equation (5.3) with the data is shown by the solid lines in figure 9. The theoretical curves do not have any free parameters other than the overall normalization, which is determined by the collection optics. The value of γ used is determined from a measurement without the dye, and the values of ℓ_a for each sample are determined from independent measurements of the transmitted intensity through the sample. The agreement between the theoretical prediction and the data is excellent, confirming the validity of our expression in equation (5.3).

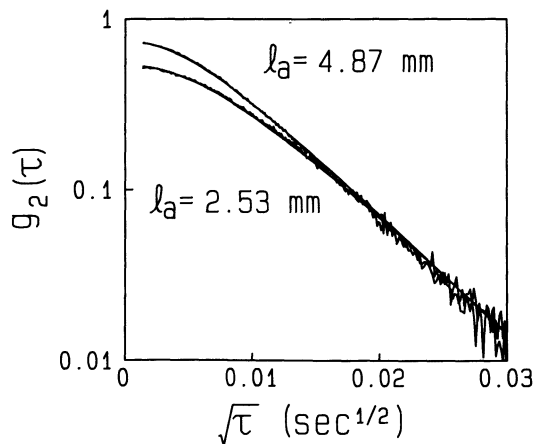


Fig. 9. — Intensity autocorrelation functions vs square root time for backscattering from samples with absorbing dye in aqueous solution. The rounding at early times is due to absorption of light which reduces the number of long light paths with contribute to the autocorrelation function.

The reduction in the contribution of long paths can also have profound effects in transmission. It can dramatically alter the functional dependence of Γ_1 on L , with Γ_1 becoming linearly dependent on L rather than L^2 . In this case, only the shortest, nearly ballistic, paths contribute to $g_1(\tau)$ in transmission with absorption, since the longer paths are attenuated. Thus the typical path contribution to the decay will have a length of L rather than $(L/\ell^*)^2 \ell^*$. However, in practice, when the absorption is sufficiently strong to significantly alter the autocorrelation function, the entire transmitted intensity will be so strongly attenuated and signal levels so low that measurements are usually impractical.

6. Polydispersity.

In many cases of interest, the scattering medium will consist of a distribution of species with different optical properties and different diffusion coefficients. Most often, this situation arises when there is a distribution of particle sizes. In the case of conventional dynamic light scattering, this leads to a non-exponential decay of the autocorrelation function. A considerable amount of research has gone into analyzing the DLS data, to invert the shape of the non-exponential autocorrelation function and obtain information about the distribution of scattering species [25]. In the case of strong multiple scattering, the decay of the autocorrelation function is already non-exponential and geometry dependent. This makes the precise consequences of polydispersity more difficult to discern from the data than in DLS. Nevertheless, these consequences can be predicted by exploiting the diffusive nature of the transport of light.

In the previous sections we have seen that the correlation function could be calculated if we knew the temporal dependence of the dephasing of a statistical path of n steps. The dephasing occurs by a random walk of phase shifts caused by the motion of the individual particles along the scattering path. For a polydisperse system the scattering from different size particles leads to phase shifts of different average magnitude resulting from the dependence of $\langle q^2 \rangle$ and D on the particle diameter. This results in a random walk with different step sizes. In the continuum limit, or diffusion approximation, the statistics the random walks reduce to simple Gaussian functions. Thus, if the step size of a random walk varies for each step, then for large n , the statistics still remain the same as for a walk with a single average step size. This is the result of the central limit theorem. Thus, the shape of the autocorrelation function should be the same for a polydisperse system as for a monodisperse system. In contrast to DLS, there should be no additional information about polydispersity in these measurements. We will only measure average properties.

To calculate the appropriate average diffusion constant for a polydisperse sample, we first consider the case of a bimodal distribution, a number density ρ_j of particles with scattering cross section σ_j and diffusion constant D_j , where $j = a, b$. We assume that there are no spatial correlations between particles of different type thus restricting our approach to $\phi < 0.1$. Then we can replace equation (2.4) for the total phase shift from an n -th order scattering process by

$$\begin{aligned} \Delta \Phi^{(n)}(\tau) &= \sum_{i=1}^n \mathbf{q}_i \cdot \Delta \mathbf{r}_i(\tau) \\ &= \sum_{i=1}^{n_a} \mathbf{q}_{a_i} \cdot \Delta \mathbf{r}_{a_i}(\tau) + \sum_{i=1}^{n_b} \mathbf{q}_{b_i} \cdot \Delta \mathbf{r}_{b_i}(\tau) \end{aligned} \quad (6.1)$$

where $n_a + n_b = n$. Since the average scattering wavevectors and root mean square displacements differ for the two species, it is convenient to sum separately over the phase

shifts for each species. The ensemble averages are calculated as in the monodisperse case but now keeping track of the species. Equation (2.5) becomes

$$G_1^{(n)}(\tau) = I_0 P(n) \left\langle e^{-q^2 \langle \Delta r_{a_i}^2(\tau) \rangle / 6} \right\rangle_q^{n_a} \left\langle e^{-q^2 \langle \Delta r_{b_i}^2(\tau) \rangle / 6} \right\rangle_q^{n_b}. \quad (6.2)$$

Performing the individual averages as before, we have

$$G_1^{(n)}(\tau) = I_0 P(n) e^{-n_a 2 k_0^2 (\ell_a / \ell_a^*) D_a \tau - n_b 2 k_0^2 (\ell_b / \ell_b^*) D_b \tau} \quad (6.3)$$

where we have left the characteristic decay times τ_{0a} and τ_{0b} in terms of D_a and D_b , the diffusion coefficients for each species, and k_0 . Thus, $\tau_{0j} = (D_j k_0^2)^{-1}$.

We must now determine the average number of scattering events from particles *a* and *b* in a path of total length *s*. The relative probabilities of scattering by *a* or *b* are proportional to their number densities and total scattering cross sections or inversely proportional to their individual mean free paths,

$$n_a / n_b = (\rho_a \sigma_a / \rho_b \sigma_b) = \ell_b / \ell_a, \quad (6.4)$$

or $n_a \ell_a = n_b \ell_b$. Substituting this into equation (6.3) gives,

$$\Delta \Phi^{(n)}(\tau) = n_a \ell_a 2 k_0^2 (D_a / \ell_a^* + D_b / \ell_b^*) \tau, \quad (6.5)$$

where the phase shift, $\Delta \Phi^{(n)}(\tau)$, is the exponent of equation (6.3). The total path length is given by *n* steps with the actual mean free path of the system ℓ' , which includes scattering from both species :

$$1/\ell' = \rho_a \sigma_a + \rho_b \sigma_b = 1/\ell_a + 1/\ell_b. \quad (6.6)$$

Since $n = n_a + n_b = n_a (1 + \ell_a / \ell_b)$, $s = n \ell' = n_a \ell_a$. For use below we also define,

$$1/\ell_{\text{eff}}^* \equiv 1/\ell_a^* + 1/\ell_b^*. \quad (6.7)$$

The final result for the time dependent dephasing from the two species is therefore :

$$\Delta \Phi^{(n)}(\tau) = s 2 k_0^2 (D_a / \ell_a^* + D_b / \ell_b^*) \tau \quad (6.8)$$

which is simply proportional to *s* and τ as expected, and has the same form as the previously derived expression for a single species. Thus, the form of the correlation functions will not change from the results for a single species provided we substitute the appropriate averages for ℓ^* and τ_0 . Writing the phase shift as :

$$\Delta \Phi^{(n)}(\tau) = (s / \ell_{\text{eff}}^*) (\tau / \tau_{\text{eff}}) \quad (6.9)$$

and generalizing to the case of many different species we have directly :

$$1/\ell_{\text{eff}}^* = \sum_j 1/\ell_j^* \quad (6.10a)$$

$$1/\tau_{\text{eff}} = 2 k_0^2 D_{\text{eff}} \quad (6.10b)$$

$$D_{\text{eff}} = \left(\sum_j D_j / \ell_j^* \right) / \left(\sum_j 1/\ell_j^* \right). \quad (6.10c)$$

The effective diffusion constant is the weighted average of the individual diffusion coefficients. Since $1/\ell_j^* = \rho_j \sigma_j^*$, the weighting factor is the number density times the

transport cross section [10] for scattering or alternatively the inverse transport mean free path for the individual species. The expressions for τ_{eff} and ℓ_{eff}^* in equation (6.10) can be directly substituted for τ_0 and ℓ^* in the correlation functions previously described. To illustrate this behavior, we measured the autocorrelation function in both transmission and backscattering from a series of binary mixtures of 0.198 μm and 0.605 μm diameter polystyrene spheres. In all cases, the functional form of the data obtained from mixtures is identical to that obtained from a single species. To compare with theory, we determine τ_{eff} for mixtures with different relative volume fractions, using backscattering measurements and assuming $\gamma = 2.1$. We calculate $1/\ell_i^* = \rho_i \sigma_i \langle 1 - \cos \phi_i \rangle$ for each species using Mie theory, and D_i from the Stokes-Einstein relation. The results are summarized in figure 10 where we compare the value of τ_{eff} determined experimentally from backscattering measurements with that calculated theoretically from D_{eff} and ℓ_{eff}^* . As can be seen, the agreement between the measured and calculated τ_{eff} is excellent.

We conclude by again emphasizing that, unlike DLS, DWS can not yield independent information about polydispersity. Instead, only average quantities can be determined. However, we can calculate the average quantities if the distribution is known which can, in principle, allow the effects of different possible distributions to be tested. One important effect that has not as yet been determined is the dependence of γ on polydispersity.

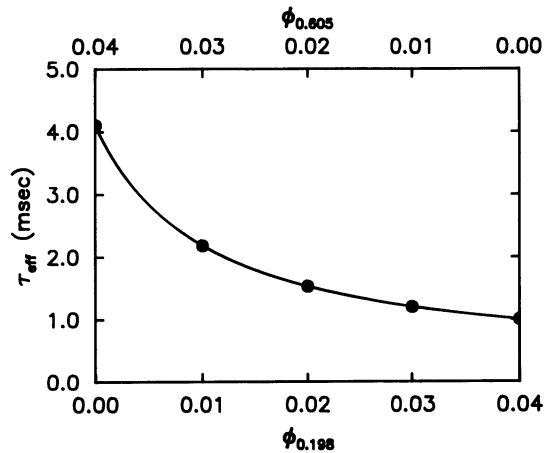


Fig. 10. — Effective decay time τ_{eff} vs volume fraction ϕ for mixtures of 0.198- μm diameter spheres and 0.605- μm -diameter spheres. The solid line through the data points is obtained using equation (6.10) where ℓ^* is determined using Mie theory as described in the text.

7. Particle sizing.

One of the most widely used and important applications of DLS is to measure particle size. Until the development of DWS, this has been limited to the regime of single scattering. DWS offers the potential of extending the use of light scattering for particle sizing to concentrated suspensions, that had previously been excluded. However, more limited information is available for particle sizing with DWS as compared to conventional DLS. For example, as shown above, no information concerning particle size polydispersity can be obtained from DWS, whereas the determination of particle size distributions is a well developed feature of DLS. Furthermore, additional information is always required to obtain τ_0 from a single

measurement of the correlation function in DWS. For a backscattering measurement, we must independently determine γ , while for transmission, we must independently determine ℓ^* , as each of these quantities enter multiplicatively with τ_0 in the appropriate expressions for the autocorrelation functions. Thus, conventional DLS is always preferable, and more powerful, for particle sizing applications. However, when multiple scattering precludes the use of DLS, DWS holds the potential for giving at least some important particle size information.

Perhaps the simplest DWS measurement for particle sizing is that of backscattering. To independently determine the value of γ , we can exploit its dependence on polarization. The autocorrelation function can be measured for both perpendicular and parallel polarizations and $\gamma_{\perp}/\gamma_{\parallel}$ can be experimentally determined. The data shown in figure 8 suggest that $\gamma_{\perp}/\gamma_{\parallel}$ is a nearly monotonic function of ℓ^*/ℓ . We plot this ratio in figure 11. Using the measured $\gamma_{\perp}/\gamma_{\parallel}$ and figure 11, we can determine the value of ℓ^*/ℓ and thereby infer the absolute values of γ_{\perp} and γ_{\parallel} . Once γ_{\perp} and γ_{\parallel} are known, τ_0 can be obtained from the decay of the individual autocorrelation functions.

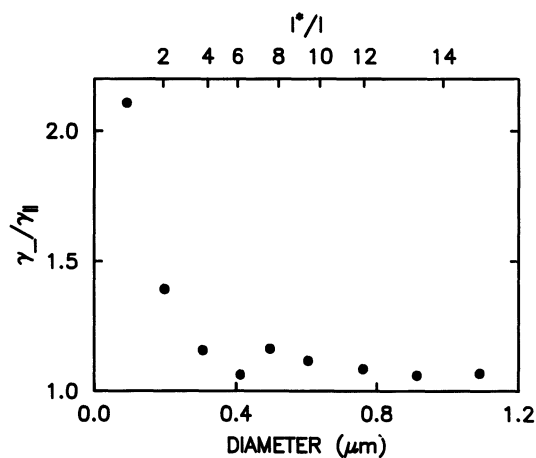


Fig. 11. — Ratio of $\gamma_{\perp}/\gamma_{\parallel}$ as a function of particle diameter and ℓ^*/ℓ .

We can also perform particle sizing using DWS with transmission measurements. In this case we must independently determine ℓ^* , which can be done most simply by measuring the static transmission. In the absence of absorption, the static transmission for an extended source is given by $(5/3) \ell^*/(L + 4 \ell^*/3)$ [10]. The value of ℓ^* for an unknown sample can most easily be determined by comparing the static transmission through it with that through the same thickness of a sample for which ℓ^* is known. It is important, however, that the sample with known ℓ^* not be too different optically from the unknown sample, to ensure that the effects of the index of refraction discontinuity at the boundaries be comparable for both samples. Then, the ratio of the transmitted intensities can be used to determine the unknown value of ℓ^* , and a measurement of the autocorrelation function will provide a measure of τ_0 and, hence, the particle size.

Each technique for DWS has its own merits. The advantages of backscattering are its simplicity in that only one optical access to the sample is required and only dynamic light scattering measurement need be made. A single measurement of the perpendicular polarization channel of the scattered light immediately provides a reasonable estimate of

τ_0 , assuming $\gamma = 2.1$. This value can be further refined through a measurement of the parallel polarization of the backscattered light. Furthermore the shape of the autocorrelation function in backscattering can provide considerable additional information. Curvature in the shape when plotted as a function of the square root of time indicates the presence of either absorption, for downward curvature at early times, or particle interactions, for upward curvature at later times [6].

Particle interactions may in fact be quite common in the concentrated suspensions for which DWS is ideally suited. When they are present, the most useful information for particle sizing purposes is the initial decay of the autocorrelation function. While this can, in principle, be determined from a backscattering measurement, in practice, the initial decay can be determined more accurately from a transmission measurement. Physically, we must determine τ_0 at very short time scales, corresponding to very small particle displacements, where the effects of the particle interactions are least important. Transmission measurements are ideally suited for this, and may be preferable for such interacting systems.

Either transmission or backscattering measurements with DWS will only provide information about an average particle size. This, of course may frequently be the most useful information, as for example, when a relatively monodisperse system is to be measured, or when the average change in a system is to be monitored. In addition, while independent information about polydispersity can not be measured, the nature of the averaging inherent in the value of τ_0 can be calculated.

8. Conclusions.

We have developed a simple theory for obtaining temporal autocorrelation functions for multiply scattered light, thereby extending the applicability of traditional dynamic light scattering to the multiple scattering regime. Our emphasis here is on the results obtained for the measured autocorrelation functions for suspensions of monodisperse Brownian particles. The key to the theory of diffusing-wave spectroscopy is the description of the transport of light within the diffusion approximation. This allows us to obtain explicit expressions for the autocorrelation function, $g_1(\tau)$, for different experimental geometries. For the transmission geometry, $g_1(\tau)$ depends on two parameters, the transport mean free path, ℓ^* , which characterizes the scattering and diffusive transport of light through the sample, and the diffusion coefficient, D , of the Brownian particles. In general, ℓ^* depends on particle size and concentration and can be determined independently by a variety of experimental measurements, including the width of the coherent backscattering cone, static transmission, and pulse propagation. Thus, if ℓ^* is known, D can be directly measured using DWS. For the backscattering geometry, $g_1(\tau)$ also depends on two parameters, the diffusion coefficient, D , and the parameter γ , which depends on particle size and the polarization state of the light. Physically, γ reflects the relative contributions of very short paths, which have not been totally depolarized. By measuring $g_1(\tau)$ for both parallel and perpendicular polarizations, both D and γ can be unambiguously determined.

In the transmission geometry, we obtain excellent agreement between experiment and the functional form for the autocorrelation function predicted by theory. In the backscattering geometry, the experimentally measured autocorrelation functions exhibit a particularly simple form when $\ell^*/\ell \gg 1$, an exponential decay with square root of time. However, our scalar theory cannot account for the observed polarization dependence. As a consequence, we introduce the additional, polarization-dependent parameters, γ_\perp and γ_\parallel .

We consider several effects that are commonly encountered in the experimental application of DWS. We show that particle polydispersity does not change the form of the measured autocorrelation functions in backscattering and transmission and that the observed decay time

can be calculated if the particle-size distribution is known. We present a simple treatment exploiting the diffusive nature of the light transport, which allows the explicit calculation of the consequences of polydispersity on the measured autocorrelation function. However, we find that the averaging inherent in the multiple scattering geometry precludes independent determination of particle size distributions. In addition, we illustrate the effects of absorption on the autocorrelation functions, and discuss how these effects can be included in the calculations.

The results of this paper demonstrate the utility of DWS in studying particle dynamics in concentrated suspensions by exploiting the strong multiple scattering that is typical in these samples. Particular applications include particle sizing through the determination of the average diffusion coefficient, and a discussion of this technique is presented. Despite the general usefulness of DWS, there still remain several important questions that must be addressed to extend the range of its applications. We do not consider the consequences of particle interactions on DWS. These can potentially be important for the concentrated suspensions that DWS can naturally be used to study. In addition, the theoretical treatment presented does not accurately deal with the very short ($s < \ell^*$), nondiffusive path present in backscattering. Their theoretical description represents an important remaining challenge for the theory of diffusive photon transport in random media and for DWS.

Acknowledgements.

We acknowledge many useful and stimulating discussions with M. J. Stephen, F. C. MacKintosh, G. Maret, and P. E. Wolf. We also thank Paul Chaikin for many useful suggestions and helpful discussions.

Appendix.

We calculate the flux of diffusing photons following the analysis of Glasstone and Edlund [21]. To this end, we first consider an infinitesimal element of area, dS , *inside the sample* in the x - y plane and calculate the diffusive flux in the positive and negative z -directions. For a sample consisting of isotropic scatterers, the number of photons which are scattered per unit time from a volume element dV in the $+z$ half-plane and reach the area element dS *without* scattering is given by :

$$\frac{Uc}{\ell} dV \frac{dS \cos \theta}{4 \pi r^2} e^{-r/\ell} \quad (\text{A.1})$$

where r is the distance between the dV and dS , and θ is the angle between r and the normal to dS (the $+z$ -axis). Since the variation in U over a distance ℓ is small, we can approximate U by a Taylor expansion to linear order :

$$U(x, y, z) = U(x_0, y_0, z_0) + (x - x_0) \left(\frac{dU}{dx} \right)_0 + (y - y_0) \left(\frac{dU}{dy} \right)_0 + (z - z_0) \left(\frac{dU}{dz} \right)_0 + \dots \quad (\text{A.2})$$

where x_0 , y_0 , and z_0 denote the coordinates of the area element, dS . To obtain the flux of photons in the $-z$ direction, we integrate equation (A.1) over the half-plane $z > z_0$ using the Taylor expansion for $U(x, y, z)$ and obtain [21]

$$J_-(z) = \frac{Uc}{4} + \frac{c\ell}{6} \frac{\partial U}{\partial z}. \quad (\text{A.3})$$

Similarly, the flux in the $+z$ direction is given by integrating over the half-plane $z < z_0$,

$$J_+(z) = \frac{Uc}{4} - \frac{c\ell}{6} \frac{\partial U}{\partial z}. \quad (\text{A.4})$$

We can rewrite these results in more general terms using the photon diffusion coefficient $D_\ell = c\ell/3$,

$$J_\pm(z) = \frac{Uc}{4} \mp \frac{D_\ell}{2} \frac{\partial U}{\partial z}. \quad (\text{A.5})$$

Within the diffusion approximation, equation (A.5) can be generalized for anisotropic scatterers by using $D_\ell = c\ell^*/3$ [21].

References

- [1] BERNE B. J. and PECORA R., *Dynamic Light Scattering: With Applications to Chemistry, Biology, and Physics* (Wiley, New York, 1976).
- [2] CLARK N. A., LUNACEK J. H. and BENEDEK G. B., *Am. J. Phys.* **38** (1970) 575.
- [3] DHONT J. K. G., in *Photon Correlation Techniques in Fluid Mechanics*, edited by E. O. Schulz-DuBois (Springer-Verlag, Berlin, 1983).
- [4] MARET G. and WOLF P. E., *Z. Phys.* **B 65** (1987) 409.
- [5] ROSENBLUH M., HOSHEN M., FREUND I. and KAVEH M., *Phys. Rev. Lett.* **58** (1987) 2754.
- [6] PINE D. J., WEITZ D. A., CHAIKIN P. M. and HERBOLZHEIMER E., *Phys. Rev. Lett.* **60** (1988) 1134.
- [7] WU X. L., PINE D. J., CHAIKIN P. M., HUANG J. S., WEITZ D. A., *J. Opt. Soc. Am.* **B 7** (1990) 15.
- [8] PHILLIES G. D. J., *Chem. Phys.* **74** (1981) 260 ;
PHILLIES G. D. J., *Phys. Rev. A* **24** (1981) 1939.
- [9] DHONT J. K. G. and DE KRUIF C. G., *J. Chem. Phys.* **79** (1983) 1658 ;
MOS H. J., PATHMAMONOHARAN C., DHONT J. K. G., DE KRUIF C. G., *J. Chem. Phys.* **84** (1986) 45.
- [10] ISHIMARU A., *Wave Propagation and Scattering in Random Media*, vol. I (Academic, New York) 1978.
- [11] VAN ALBADA M. P. and LEGENDIJK A., *Phys. Rev. Lett.* **55** (1985) 2692.
- [12] WOLF P. E. and MARET G., *Phys. Rev. Lett.* **55** (1985) 2696.
- [13] IOFFE A. F. and REGEL A. R., *Prog. Semicond.* **4** (1960) 237.
- [14] GOLUBENTSEV A. A., *Zh. Eksp. Teor. Fiz.* **86** (1984) 47 [*Sov. Phys. JETP* **59** (1984) 26].
- [15] STEPHEN M. J., *Phys. Rev.* **B 37** (1988) 1.
- [16] MACKINTOSH F. C. and JOHN S., *Phys. Rev.* **B 40** (1989) 2383.
- [17] PINE D. J., WEITZ D. A., MARET G., WOLF P. E., CHAIKIN P. M. and HERBOLZHEIMER E., in *Classical Localization of Waves*, edited by P. Sheng, World Scientific (1990).
- [18] WOLF P. E., MARET G., AKKERMANS E. and MAYNARD R., *J. Phys. France* **49** (1988) 63.
- [19] The derivation of the expression for $J_+(z_0)$ in (Eq. (2.19)) assumes that U and its spatial derivatives are finite and well-defined for $z \leq z_0$. Since these conditions are not met for $z_0 = 0$, the validity of setting $J_+ = 0$ at $z = 0$ is open to question ; we prefer to avoid making this assumption.
- [20] We also note that other approximate boundary conditions are possible within the diffusion approximation. A frequently used alternative boundary condition is to use the exact Milne solution for isotropic scatterers and set U equal to zero at an « extrapolation length » outside the sample, usually taken to be $0.7104 \ell^*$ (see Ref. [10]). The boundary conditions we use (in

Eq. (2.20)) are consistent with an extrapolation length of $2/3 \ell^*$. Fortunately, the nature of the solutions to the diffusion equation do not depend sensitively on the boundary conditions used in many geometries of experimental interest. Nevertheless, for certain experiments, notably in backscattering, the exact nature of the boundary conditions can affect the solutions one obtains.

- [21] GLASSTONE S. and EDLUND M. C., *The Elements of Nuclear Reactor Theory* (D. Van Nostrand Co., Princeton, New Jersey) 1952.
- [22] CARSLAW H. S. and JAEGER J. C., *Conduction of Heat in Solids*, 2nd ed. (Clarendon, Oxford) 1959. Solutions to the diffusion equation for an extremely wide variety of initial and boundary conditions can be found in this classic text. In the present context, chapters 12 and 14, which use Laplace transform and Green's functions techniques, are particularly valuable.
- [23] PINE D. J., WEITZ D. A., CHAIKIN P. M. and HERBOLZHEIMER E., in *Proceedings of the Topical Meeting on Photon Correlation Techniques and Applications*, edited by A. Smart and J. Abbiss. (Optical Society of America, Washington, 1988).
- [24] MACKINTOSH F. C., ZHU J. X., PINE D. J. and WEITZ D. A., *Phys. Rev.* **B 40** (1989) 9342.
- [25] See, for example, articles by OSTROWSKY N. and SORNETTE D. or BERTERO M. and PIKE E. R. in *Photon Correlation Techniques in Fluid Mechanics*, edited by E. O. Schulz-DuBois (Springer-Verlag, Berlin, 1983).